Electronic Supplementary Material (ESI) for ChemComm.

Unambiguous localization of titanium and iron cations in doped manganese hollandite nanowires

Isabel Gómez-Recio[a,b], Alberto Azor-Lafarga[a], M.Luisa Ruiz-González[a], María Hernando[a], Marina Parras[a], José Juan Calvino[c], María Teresa Fernández-Díaz[d], David Portehault[b], Clement Sanchez[b], and José M. González-Calbet[a,e*]

[a] Departamento de Química Inorgánica, Facultad de Químicas, Universidad Complutense, 28040-Madrid, Spain.
[b] Sorbonne Université, CNRS, Collège de France, Laboratoire Chimie de la Matière Condensée de Paris (LCMCP), 4 Place Jussieu, F-75005 Paris, France.
[c] Facultad de Ciencias, Universidad de Cádiz, Campus Rio San Pedro, Puerto Real, Spain.
[d] *Institut Laue-Langevin, 71 avenue des Martyrs, CS 20156, 38042 Grenoble cedex 9, France*
[e] Centro Nacional de Microscopía Electrónica, Universidad Complutense, 28040 Madrid, Spain.

SI 1. Synthesis

In a typical one-pot synthesis, 30 mL of a solution of $Mn(SO_4)_2$ (1.60 M, 98%, Sigma-Aldrich) and HNO_3 (1.28 M, 65% w.w. Sigma-Aldrich) are added dropwise, under vigorous stirring, over 100 mL of a solution of $KMnO_4$ (90.4 M, 9%, Sigma-Aldrich). The suspension is stirred and refluxed over 24 h. After filtration, the precipitate is washed with Mili-Q water and dried overnight at 323 K.

In the two steps route, birnessite oxide is synthesized as follows: 30 mL of a solution of $Mn(NO_3)_2{\cdot}4H_2O$ (1 M, 97%, Sigma-Aldrich) are quickly injected directly over the vortex of a vigorously stirred mixture of a solution of KOH (300 mL, 0.8 M, 99%, Sigma-Aldrich) and of H_2O_2 (6 mL, 33% w.w. Sigma-Aldrich). A dark brown precipitate forms immediately. After 10 min, the solid is recovered by centrifugation, washed with Mili-Q water and dried overnight at 323 K. The second step of this synthetic pathway allows obtaining hollandite oxides, according to the following procedure: 1.5 g of doped or undoped birnessite oxide are loaded into a 116 mL Teflon-lined stainless steel autoclave with a solution of KCl (58 mL, 1 M, 99.99% Sigma Aldrich) and of H_2SO_4 (0.5 M, 95%, Sigma-Aldrich). The mixture is heated at 398 K for 24 h. The precipitate is washed and dried as described above.

Dopant	Synthetic pathway			
	One – pot		Two-Steps	
	$Mn(SO_4)_2$:dopant molar ratio	Composition (EPMA)*	$Mn(NO_3)_2$:dopant molar ratio	Composition (EPMA*)
	1 : 0	$K_{0.12}MnO_{\square}$	1 : 0	$K_{0.12}MnO_{\square}$
Ti	0.95 : 0.05	$K_{0.10}Mn_{0.93}Ti_{0.07}O_{\square}$	0.95 : 0.05	$K_{0.11}Mn_{0.92}Ti_{0.08}O_{\square}$
	0.90 : 0.10	$K_{0.08}Mn_{0.85}Ti_{0.15}O_{\square}$	0.85 : 0.15	$K_{0.10}Mn_{0.82}Ti_{0.18}O_{\square}$
Fe	0.95 : 0.05	$K_{0.12}Mn_{0.95}Fe_{0.05}O_{\square}$	0.95 : 0.05	$K_{0.12}Mn_{0.96}Fe_{0.04}O_{\square}$
	0.80 : 0.20	$K_{0.07}Mn_{0.86}Fe_{0.14}O_{\square}$	0.80 : 0.20	$K_{0.10}Mn_{0.84}Fe_{0.16}O_{\square}$

Table SI 1. Chemical composition of doped hollandites and the corresponding initial ratio of reagents.

*Experimental error of this technique is 1%

SI 2. Powder X-Ray Diffraction

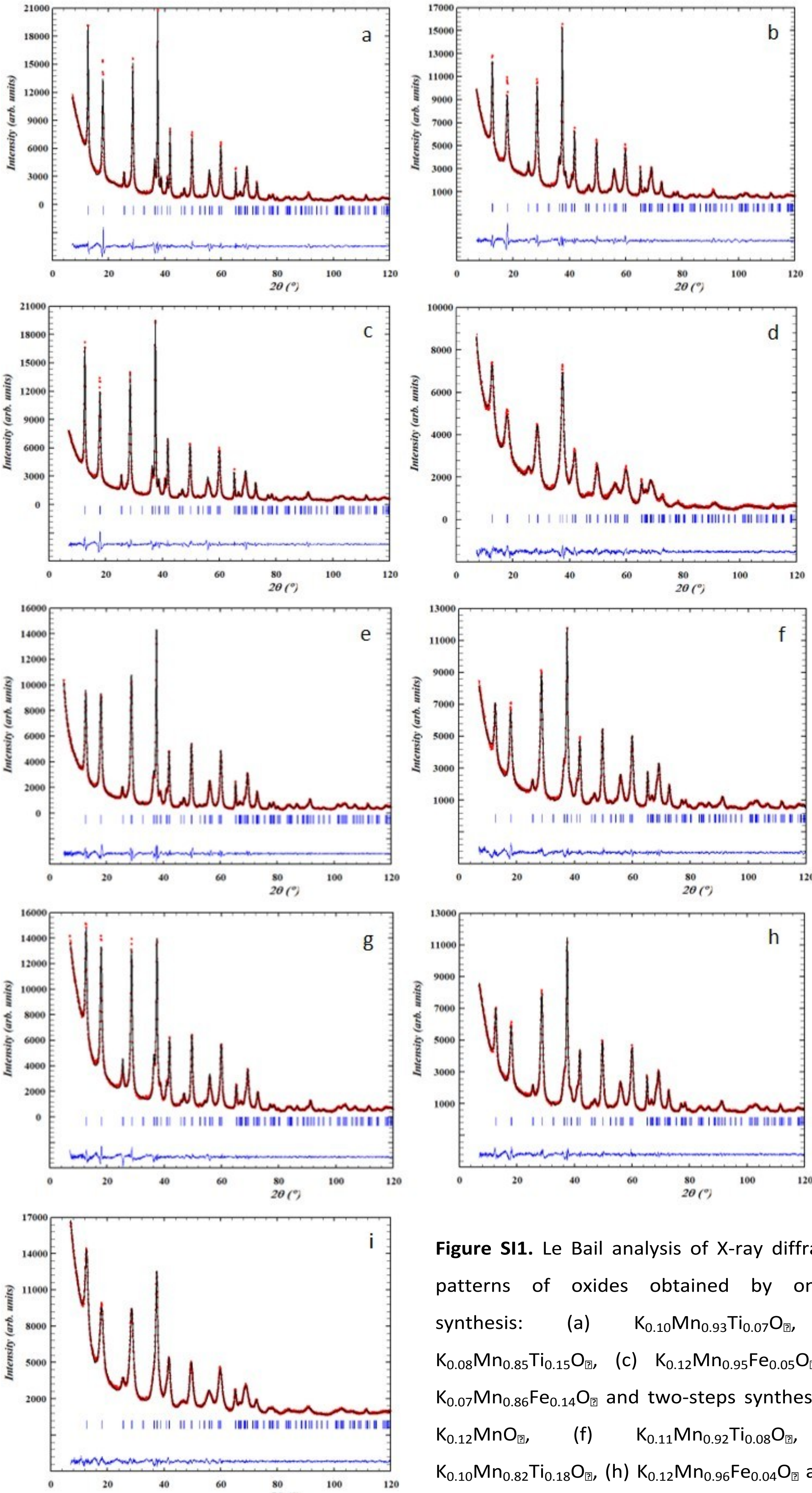

Figure SI1. Le Bail analysis of X-ray diffraction patterns of oxides obtained by one-pot synthesis: (a) $K_{0.10}Mn_{0.93}Ti_{0.07}O_{\square}$, (b) $K_{0.08}Mn_{0.85}Ti_{0.15}O_{\square}$, (c) $K_{0.12}Mn_{0.95}Fe_{0.05}O_{\square}$, (d) $K_{0.07}Mn_{0.86}Fe_{0.14}O_{\square}$ and two-steps synthesis: (e) $K_{0.12}MnO_{\square}$, (f) $K_{0.11}Mn_{0.92}Ti_{0.08}O_{\square}$, (g) $K_{0.10}Mn_{0.82}Ti_{0.18}O_{\square}$, (h) $K_{0.12}Mn_{0.96}Fe_{0.04}O_{\square}$ and (i) $K_{0.10}Mn_{0.84}Fe_{0.16}O_{\square}$.

Table SI 2. Cell parameters of hollandite manganese oxides provided by Le Bail analysis of XRD patterns.

One – pot				Two-Steps			
	a (Å)	c (Å)	Chi2		a (Å)	c (Å)	Chi2
$K_{0.12}MnO_{\square}$	9.8326(4)	2.85080(9)	2.33	$K_{0.12}MnO_{\square}$	9.8136(3)	2.85380(7)	3.87
$K_{0.10}Mn_{0.93}Ti_{0.07}O_{\square}$	9.8672(3)	2.85719(6)	6.01	$K_{0.11}Mn_{0.92}Ti_{0.08}O_{\square}$	9.8682(2)	2.85821(6)	2.64
$K_{0.08}Mn_{0.85}Ti_{0.15}O_{\square}$	9.8824(4)	2.85948(8)	4.98	$K_{0.10}Mn_{0.82}Ti_{0.18}O_{\square}$	9.8645(3)	2.85998(7)	3.35
$K_{0.12}Mn_{0.95}Fe_{0.05}O_{\square}$	9.8533(3)	2.85509(6)	5.66	$K_{0.12}Mn_{0.96}Fe_{0.04}O_{\square}$	9.8511(3)	2.85787(7)	2.54
$K_{0.07}Mn_{0.86}Fe_{0.14}O_{\square}$	9.8365(8)	2.8543(2)	2.19	$K_{0.10}Mn_{0.84}Fe_{0.16}O_{\square}$	9.8718(5)	2.86122(1)	2.60

Table SI 3. Crystal domain length along the [001] direction of hollandite oxides.

d_{001} (Å)	
$K_{0.12}MnO_{\square}$	23.1
$K_{0.11}Mn_{0.92}Ti_{0.08}O_{\square}$	20.6
$K_{0.10}Mn_{0.82}Ti_{0.18}O_{\square}$	15.4
$K_{0.12}Mn_{0.96}Fe_{0.04}O_{\square}$	19.0
$K_{0.10}Mn_{0.84}Fe_{0.16}O_{\square}$	8.0

SI 3. Powder Neutron Diffraction

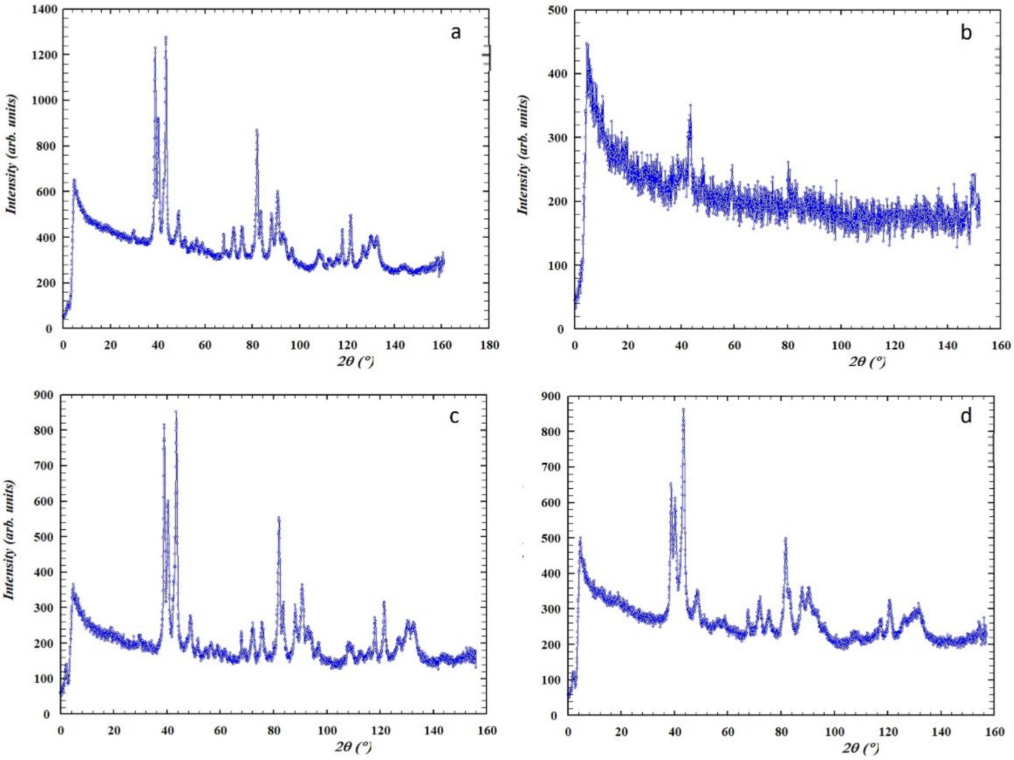

Figure SI 2. Neutron powder diffraction patterns of hydrated hollandite oxides, (a) undoped hollandite, (b) iron doped hollandite, partially dehydrated (c) undoped and (d) iron doped hollandites. The signal-to-noise ratio is very low for the hydrated samples (a, b) because of inelastic scattering by remaining water molecules. These data are then not reliable for structural refinement and the samples were dehydrated prior to neutron diffraction acquisition (Figure SI 3).

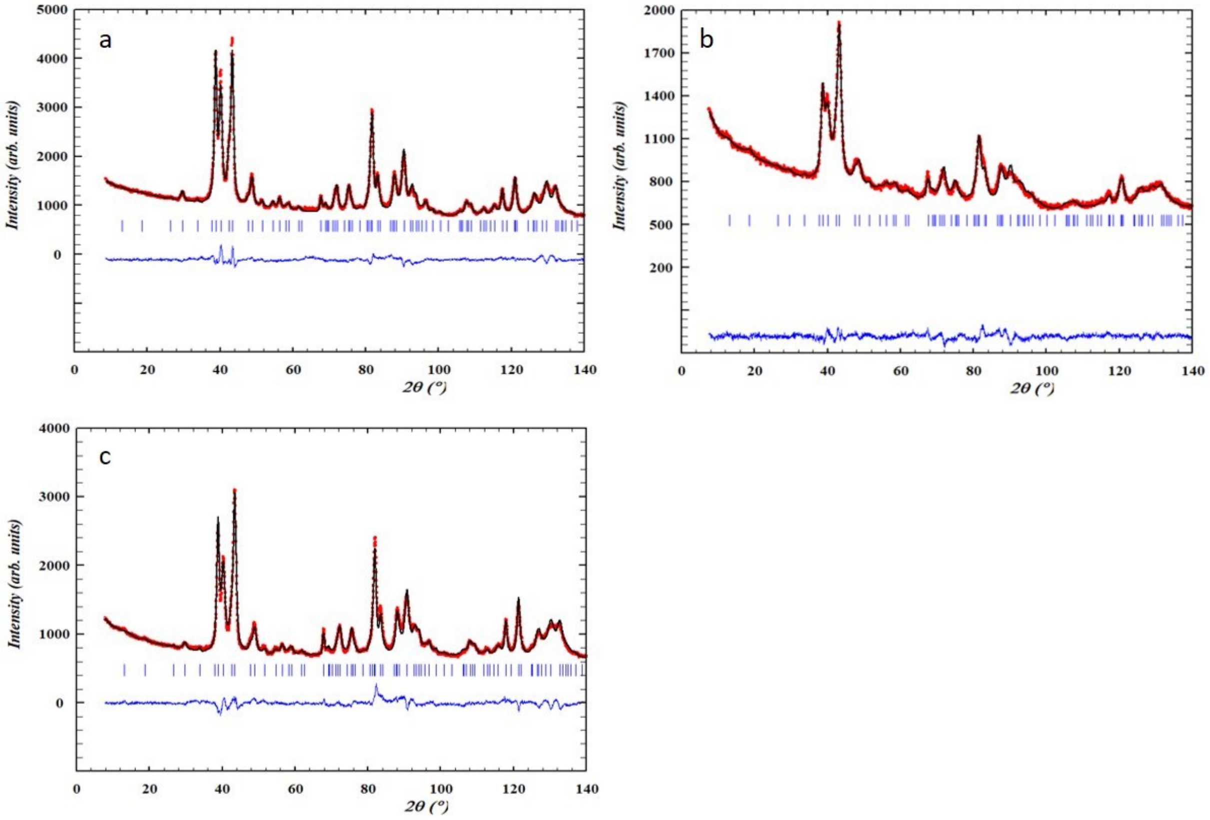

Figure SI 3. Rietveld refined ND patterns of (a, b) iron doped and (c) titanium doped hollandites.

The pretreatment at 180 °C carried out before the ND measurements gives rise to partial dehydration of the samples. The high background observed in the neutron diffraction pattern can be associated to the incoherent scattering of hydrogen from water molecules present in hollandites. Actually, the weak and spread negative scattering found in the K site and around this position observed in the difference Fourier map of the $K_{0.11}MnO_2$, Figure SI 4, could correspond, according to B. Ouladdiaf *et al.*[1], to scattering from water molecules (or H_3O^+), which have negative average scattering length. Herein we show that without including this factor in the Rietveld refinement, all samples described here are only partially dehydrated and may include disordered H_2O or H_3O^+ in the 2x2 tunnels.

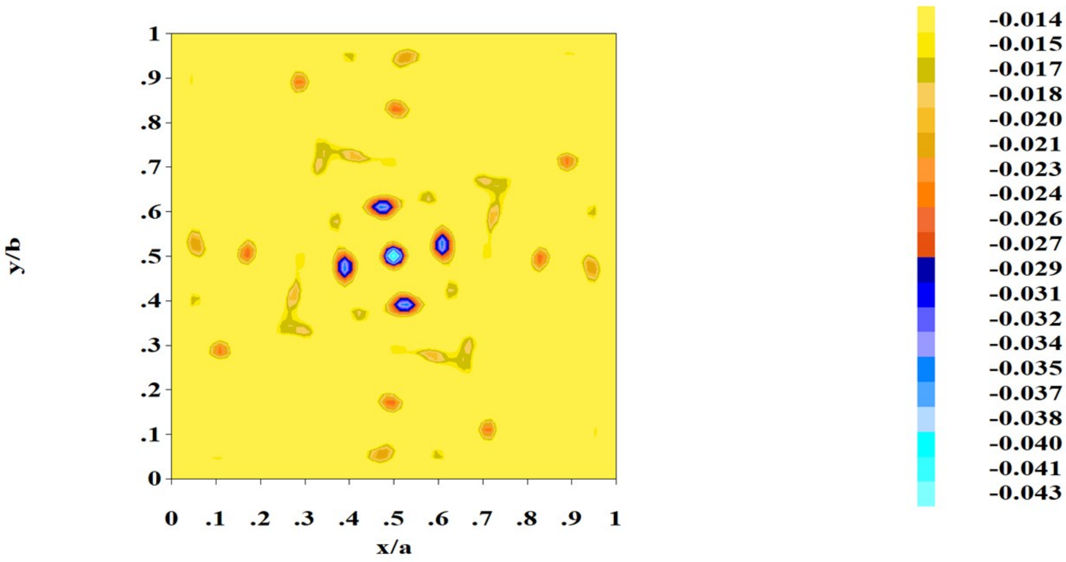

Figure SI 4. Difference Fourier map for neutron scattering density of the section z = 0 calculated from the structural model proposed for $K_{0.11}MnO_{2-\delta}$. The residual negative scattering can be associated to water molecules.

Table SI 4. Structural parameters of hollandite oxides obtained from neutron diffraction Rietveld analysis.

	$K_xMn_{1-y}Fe_yO_{2-\delta}$			$K_xMn_{0.85}Ti_{0.15}O_{2-\delta}$
	y = 0	y = 0.05	y = 0.20	
Composition	$K_{0.11}MnO_{1.958(12)}$	$K_{0.11}Mn_{0.946(2)}Fe_{0.054(2)}O_{1.899(14)}$	$K_{0.09}Mn_{0.844(2)}Fe_{0.156(2)}O_{1.904(17)}$	$K_{0.1}Mn_{0.82}Ti_{0.18}O_{1.964(8)}$
a=b (Å)	9.8099(2)	9.8140(3)	9.8659(7)	9.8404
c (Å)	2.85354(5)	2.85555(6)	2.865688(16)	2.86085(5)
Boverall		1.51(2)	1.07(2)	0.85342
R_B	5.75	7.16	4.85	4.68
R_p	2.71		1.55	2.06
R_{wp}	3.50	3.51	2.05	2.70
χ^2	2.54	7.86	2.42	5.92
Mn/M (x, y, 0)				
X	0.3489(4)	0.3468(5)	0.3454(13)	0.3472(3)
Y	0.1661(4)	0.1673(5)	0.1709(1)	0.1660(3)
Occ Mn/M	1	0.946(2)/0.054(2)	0.844(2)/0.155(2)	0.82/0.18
Biso	0.61(4)			
K (0, 0, 0.5)				
Occ	0.48	0.48	0.40	0.40
Biso	3.7(6)			
O1 (x, y, 0)				
X	0.1535(4)	0.1512(3)	0.1504(3)	0.1523(2)
Y	0.2026(2)	0.1693(4)	0.1711(5)	0.20239(17)
B_{iso}	0.687(14)			
occ	1	1	1	1
O2 (x, y, 0)				
X	0.5418(3)	0.5410(3)	0.5411(3)	0.5423(2)
Y	0.1664(4)	0.1693(4)	0.1711(5)	0.1668(3)
occ	0.958(12)	0.90(2)	0.90(2)	0.96(4)
B_{iso}	0.687(14)			

Table SI 5. Selected interatomic distances (Å) in hollandite oxides.

	$KxMn_{1-y}Fe_yO_{2-\delta}$			$K_{0.1}Mn_{0.85}Ti_{0.15}O_{2-\delta}$
	y= 0	y = 0.05	y = 0.20	y = 0.15
M-O1	1.951(5)	1.951(6)	1.949(13)	1.951(4)
M-O1	1.922(3)x2	1.913(3)x2	1.901(7)x2	1.929(3)x2
M-O2	1.891(5)	1.906(6)	1.930(13)	1.920(3)
M-O2	1.883(3)x2	1.89884)x2	1.929(8)x2	1.884(3)x2
M-M edge-sharing	2.853(5) 2.919(5)	2.877(6) 2.856(1)	2.8657(2) 2.834(15)	2.904(4) 2.8609(1)
M-M corner-sharing	3.426(5)	3.458(6)	3.520(17)	3.451(4)

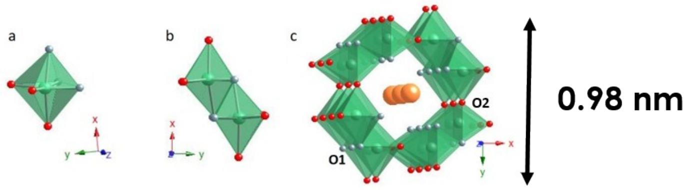

Figure SI 5. Schematic drawing of (a) MO_6 octahedra, (b) edge-sharing octahedral and (c) crystal structure of hollandite oxide. Color code: K orange, M green, grey O1 and red O2.

SI 4. Transmission Electron Microscopy (TEM)

A preliminary TEM study at low and medium magnification was performed with a JEOL 2100 transmission electron microscope, equipped with an EDS (OXFORD INCA) spectrometer, in order to study the morphology, size and average composition of the hollandite samples.

High Resolution Transmission Electron Microscopy (HRTEM) images of undoped samples were mainly obtained in a JEOL-JEM GRAND ARM 300cF microscope equipped with a Cs Corrector (ETA-JEOL). A precise measurement of the aberrations and an optimized correction was done using the corrector control software JEOL COSMO. The final values of the aberration coefficients are collected in Table SI.6. The accelerating voltage was set to 60 kV in order to minimize the sample damage. The HRTEM images were acquired using a CMOS camera (4096 x 4096 pixels, Gatan OneView).

Table SI 6. Aberration coefficients obtained after the measurement and correction of aberrations at 60 kV acceleration voltage

Aberration Coefficients	Value
O2 (Defocus)	-104.78 nm
A2(Twofold astigmatism)	0.958 nm
P3 (Axial coma)	79,236 nm
A3 (Three fold astigmatism)	22.814 µm
O4 (Spherical aberration)	1.280 µm

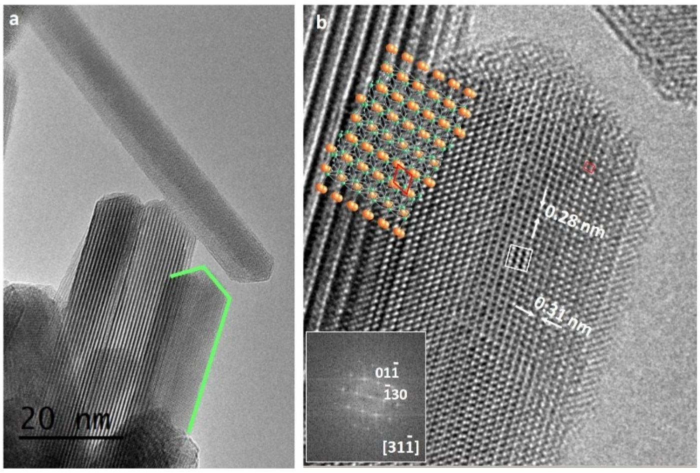

Figure SI 6. (a) TEM image showing typical elongated particles in the undoped hollandite (b) HRTEM image of the particle marked in green in *a* and its corresponding FFT at the left bottom side. The calculated image is inserted (squared area), taking into account the hollandite atomic sites and the microscope experimental conditions for Δt=5 nm and Δf=-20 nm, along the [31-1] zone axis. A schematic model of the structure along the [31-1] projection has been also included.

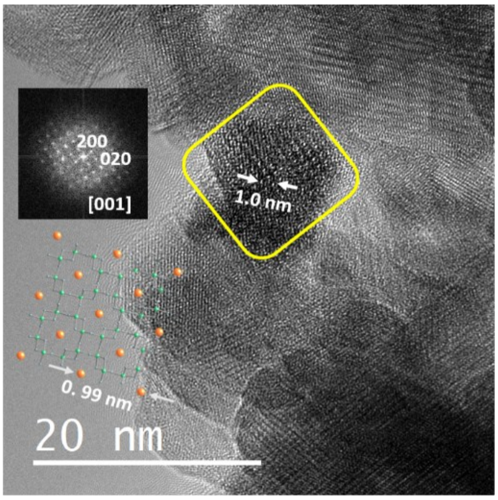

Figure SI 7. Representative HRTEM image, obtained in a JEOL 300 cFEG microscope, of an iron-doped hollandite showing the presence of nanoparticles in different orientations. Since the particle size decreases when the dopant is introduced, particles along the [001] zone axis are now visible, as the one highlighted in this image. The FFT corresponding to the particle oriented along [001] is included as well as a schematic model of the hollandite structure along this direction.

SI. 5 Scanning Transmission electron microscopy (STEM) and Electron Energy Loss Spectroscopy (EELS) for local compositional analysis

This study has been performed in a probe spherical aberration corrected microscope JEOL JSM-ARM200F (Cold Emission Gun). According to preliminary studies in these hollandite compounds, the microscope was operated at 80 kV using a low current emission density in order to minimize the damage of the samples (probe size ~0.08 nm). Inner and outer collection semiangles of 68 and 280 mrad were set for the acquisition of atomically resolved HAADF images. The microscope is equipped with a GIF-QuantumERTM spectrometer, used for the EELS experiments (with a collection semiangle of 18 mrad and a convergence semiangle of 20.3 mrad). EELS chemical maps allow us to confirm and localize the metal elements of the hollandites. They were acquired with a spatial resolution of ~0.08 nm over a total acquisition time of 1 minute with an energy dispersion of 0.4 eV per channel. In order to study the oxidation states of the transition metals, ELNES spectra were acquired using the spectrum line mode, with an energy dispersion of 0.25 eV per channel and an acquisition time of 0.5 s over an average total number of 40 to 100 points (depending on the number of layers) and with a pixel size of 1.5 Å. EELS Principal component analysis was always performed on EELS data set to de-noise the spectra by using the MSA plug-ins for Gatan DMS analysis toolbox[2]. The zero loss peak was simultaneously acquired (10-5 s) using Dual EELS, meaning that the experimental signal is perfectly aligned and calibrated. The identification of the Mn, Fe, Ti oxidation states was done by comparison with standards for the different oxidation states: Mn^{2+} ($CaMnO_2$), Mn^{3+}($LaMnO_3$) and Mn^{4+} ($Ca_2Mn_3O_8$), Fe^{2+} ($FeTiO_3$), Fe^{3+}(Fe_2O_3), Ti^{3+} (Ti_2O_3) and Ti^{4+} (TiO_2). The comparison was done by two approaches: i) comparison of the edge positions for all the metal transitions and ii) comparison of the relative intensity of the M-L_2 and M-L_3 (M= Mn, Fe) white lines. The M-L_2 and M-L_3 relative intensities were obtained, using the Gatan GMS2 software, by fitting the positive component of the second derivate of the M-$L_{2,3}$ white lines to a Gaussian curve and calculating the area under the curve.

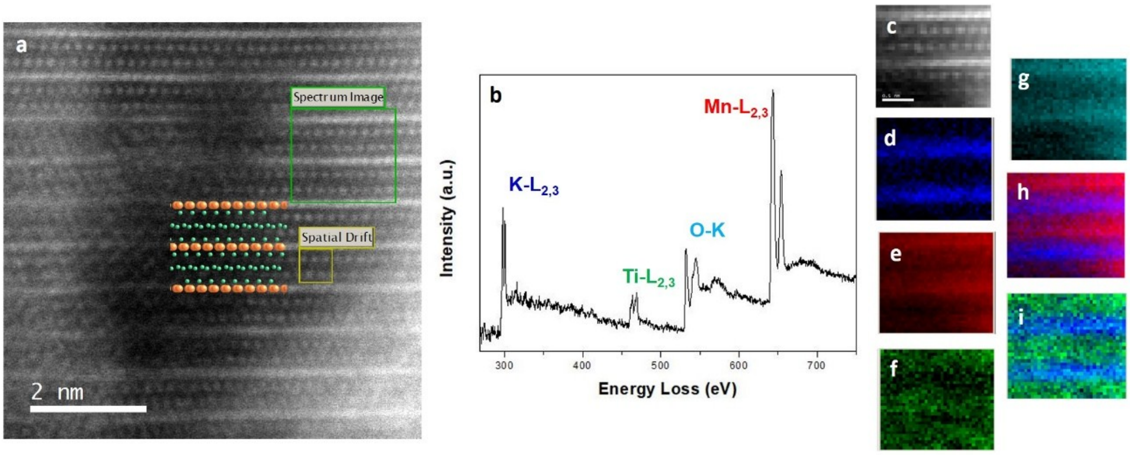

Figure SI 8. STEM-EELS study of Ti-doped hollandites. (a) HAADF images along the [111] zone axis, indicating the area where the spectrum image was acquired; a schematic representation of the structure is also included. The area of the image used to automatically avoid spatial drift of the sample during Dual EELS acquisition is also marked. (b) Sum spectrum showing the edge of all the elements present. (c) HAADF image simultaneously recorded with the spectra. (d-g) Chemical maps obtained from the different signals (Mn red, K blue, Ti green, O soft blue). (h) Combined map corresponding to K and Mn. (i) Combined map corresponding to K and Ti.

EELS study for the identification of Mn, Fe and Ti oxidation states

Comparison of the energy loss position of the Mn-$L_{2,3}$, M-$L_{2,3}$ (M=Fe and Ti) signals of $K_{0.09}Mn_{0.88}Fe_{0.12}O_\delta$ and $K_{0.11}Mn_{0.92}Ti_{0.08}O_\delta$, Comparison of the energy loss position of the Mn-$L_{2,3}$, M-$L_{2,3}$ (M=Fe and Ti) signals of $K_{0.09}Mn_{0.88}Fe_{0.12}O_\delta$ and $K_{0.11}Mn_{0.92}Ti_{0.08}O_\delta$, respectively with references.

$K_{0.09}Mn_{0.88}Fe_{0.12}O_{\delta}$

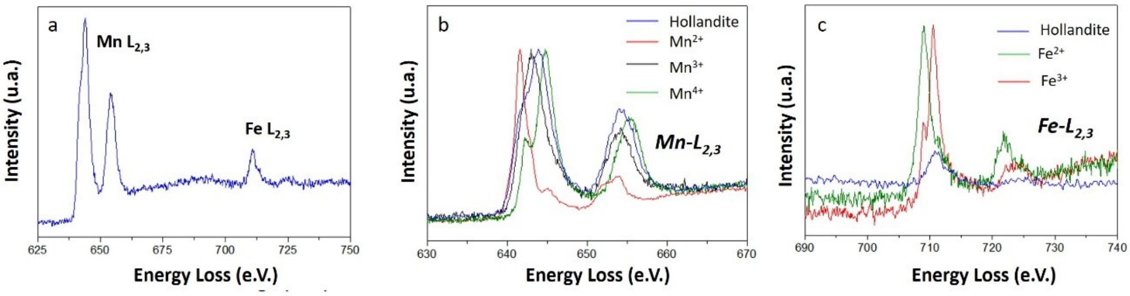

Figure SI 9. (a) EELS spectra obtained along a line showing the coexistence of Mn and Fe; (b) Mn-$L_{2,3}$ edge in comparison with references evidencing the presence of Mn^{3+} and Mn^{4+}; (c) Fe-$L_{2,3}$ edge in comparison with references suggesting the presence of Fe^{3+}.

$K_{0.11}Mn_{0.92}Ti_{0.08}O_{\delta}$

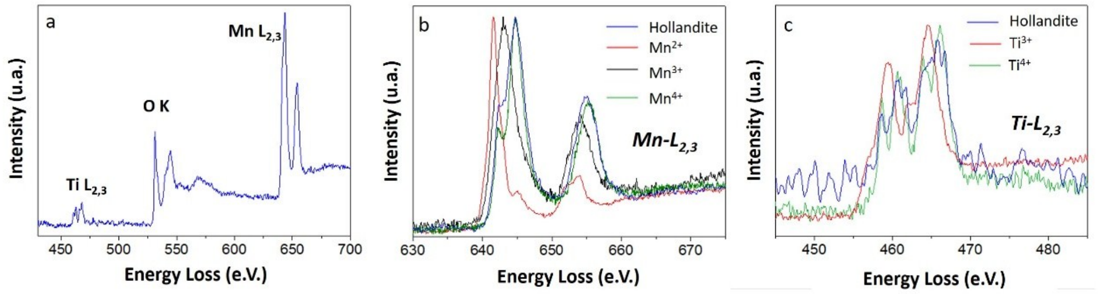

Figure SI 10. (a) EELS spectra obtained along a line showing the coexistence of Mn and Ti; (b) Mn-$L_{2,3}$ edge in comparison with references evidencing the presence of Mn^{3+} and Mn^{4+}; (c) Ti-$L_{2,3}$ edge in comparison with references suggesting the presence of Ti^{4+}.

Table SI 7. Experimental intensity ratios $I(L_3/L_2)$ for Mn in $K_{0.09}Mn_{0.88}Fe_{0.12}O_{\delta}$, $K_{0.11}Mn_{0.92}Ti_{0.08}O_{\delta}$ and $I(L_3/L_2)$ for Fe in $K_{0.09}Mn_{0.88}Fe_{0.12}O_{\delta}$. The results indicate the presence of Mn^{3+} and Mn^{4+} in the three doped samples as well as Fe^{3+} in the Fe doped samples in agreement with the energy position shown in previous Figures SI.5 and SI.6.

	$I(L_3/L_2)$ Mn	$I(L_3/L_2)$ Fe
$K_{0.09}Mn_{0.88}Fe_{0.12}O_{\delta}$	1.9 ±0.1	5.3±0.1
$K_{0.11}Mn_{0.92}Ti_{0.08}O_{\delta}$	2.0 ±0.1	5.3±0.1
$Ca_2Mn_3O_8$ (Mn^{4+})	1.8 ±0.1	
$LaMnO_3$ (Mn^{3+})	2.4 ±0.1	
$CaMnO_2$ (Mn^{2+})	4.6±0.1	
Fe_2O_3 (Fe^{3+})		4.6±0.1
$FeTiO_3$ (Fe^{2+})		3.9±0.1

1. B. Ouladdiaf, J. Rodríguez-Carvajal, C. Goutaudier, S. Ouladdiaf, B. Grosgogeat, N. Pradelle and P. Colon, *Materials Research Express*, 2015, **2**, 025401.
2. M. Watanabe, E. Okunishi and K. Ishizuka, *Microscopy and Analysis*, 2009, **23**, 5-7.